

# Black TiO<sub>2</sub> nanoprobe-mediated mild phototherapy reduces intracellular lipid levels in atherosclerotic foam cells via cholesterol regulation pathways instead of apoptosis

Ting Dai<sup>a,1</sup>, Wenming He<sup>a,1</sup>, Shuangshuang Tu<sup>a,b</sup>, Jinru Han<sup>b,c,d</sup>, Bo Yuan<sup>b,d</sup>,  
Chenyang Yao<sup>b,d</sup>, Wenzhi Ren<sup>b,d,\*\*</sup>, Aiguo Wu<sup>b,d,\*</sup>

<sup>a</sup> Department of Cardiology, The Affiliated Hospital of Medical School, Ningbo University, 247 Renmin Road, Jiangbei District, Ningbo, Zhejiang Province, 315020, China

<sup>b</sup> Cixi Institute of Biomedical Engineering, International Cooperation Base of Biomedical Materials Technology and Application, CAS Key Laboratory of Magnetic Materials and Devices & Zhejiang Engineering Research Center for Biomedical Materials, Ningbo Institute of Materials Technology and Engineering, Chinese Academy of Sciences, 1219 ZhongGuan West Road, Ningbo, 315201, China

<sup>c</sup> University of Chinese Academy of Sciences, No. 1 Yanqihu East Road, Huairou District, Beijing, 101408, China

<sup>d</sup> Advanced Energy Science and Technology Guangdong Laboratory, Huizhou, 516000, China

## ARTICLE INFO

### Keywords:

Atherosclerosis  
Black TiO<sub>2</sub> nanoparticles  
Phototherapy  
Cholesterol homeostasis

## ABSTRACT

Given that apoptosis increases the risk of plaque rupture, strategies that reduce intracellular lipid levels without killing foam cells are warranted for safe and effective treatment of atherosclerosis. In this study, a mild phototherapy strategy is carried out to achieve the hypothesis. Foam cell-targeted nanoprobes that allow photothermal therapy (PTT) and/or photodynamic therapy (PDT) were prepared by loading hyaluronan and porphyrin onto black TiO<sub>2</sub> nanoparticles. The results showed that when temperatures below 45 °C, PTT alone and PTT + PDT significantly reduced the intracellular lipid burden without inducing evidently apoptosis or necrosis. In contrast, the use of PDT alone resulted in only a slight reduction in lipid levels and induced massive apoptosis or necrosis. The protective effect against apoptosis or necrosis after mild-temperature PTT and PTT + PDT was correlated with the upregulation of heat shock protein 27. Further, mild-temperature PTT and PTT + PDT attenuated intracellular cholesterol biosynthesis and excess cholesterol uptake via the SREBP2/LDLR pathway, and also triggered ABCA1-mediated cholesterol efflux, ultimately inhibiting lipid accumulation in foam cells. Our results offer new insights into the mechanism of lipid regulation in foam cells and indicate that the black TiO<sub>2</sub> nanoprobes could allow safer and more effective phototherapy of atherosclerosis.

## 1. Introduction

Atherosclerosis (AS) is a chronic cardiovascular disease that poses a serious threat to human health and life. AS is characterized by excessive lipid accumulation in arterial walls, immunocytes infiltration, and fibrous caps formation [1,2]. Currently, drug-based therapies that reduce blood lipid levels are routinely used for AS treatment [3].

However, these drugs can sometimes cause adverse effects, for example, lipid-regulating drugs such as statins are known to cause impaired liver function. Consequently, safe and effective therapeutic methods are required for inhibiting the development of AS. Macrophages are the most abundant cells in atherosclerotic plaques and are therefore involved in key processes associated with AS development. Macrophages can internalize lipids and transform them into foam cells,

Peer review under responsibility of KeAi Communications Co., Ltd.

\*\* Corresponding author. Cixi Institute of Biomedical Engineering, International Cooperation Base of Biomedical Materials Technology and Application, CAS Key Laboratory of Magnetic Materials and Devices & Zhejiang Engineering Research Center for Biomedical Materials, Ningbo Institute of Materials Technology and Engineering, Chinese Academy of Sciences, 1219 ZhongGuan West Road, Ningbo, 315201, China.

\* Corresponding author. Cixi Institute of Biomedical Engineering, International Cooperation Base of Biomedical Materials Technology and Application, CAS Key Laboratory of Magnetic Materials and Devices & Zhejiang Engineering Research Center for Biomedical Materials, Ningbo Institute of Materials Technology and Engineering, Chinese Academy of Sciences, 1219 ZhongGuan West Road, Ningbo, 315201, China.

E-mail addresses: [renwzh@nimte.ac.cn](mailto:renwzh@nimte.ac.cn) (W. Ren), [aiguo@nimte.ac.cn](mailto:aiguo@nimte.ac.cn) (A. Wu).

<sup>1</sup> Ting Dai and Wenming He contributed equally to this work.

<https://doi.org/10.1016/j.bioactmat.2022.01.013>

Received 7 November 2021; Received in revised form 8 December 2021; Accepted 10 January 2022

Available online 17 January 2022

2452-199X/© 2022 The Authors. Publishing services by Elsevier B.V. on behalf of KeAi Communications Co. Ltd. This is an open access article under the CC BY-NC-ND license (<http://creativecommons.org/licenses/by-nc-nd/4.0/>).

increasing the risk of plaque rupture and ultimately causing stroke or myocardial infarction [4,5]. Therefore, foam cells could be a promising anti-AS therapeutic target.

With the development of nanotechnology, nanoparticle-based phototherapy has received increasing attention for its potential in the treatment of AS. Phototherapy mainly includes photothermal therapy (PTT) and photodynamic therapy (PDT), and it offers advantages such as accurate spatial selectivity, minimal invasiveness, and convenient operation. During phototherapy, photosensitizers or photothermal agents are phagocytized by cells. These agents generate reactive oxygen species (ROS) or heat after irradiation with near-infrared (NIR) light, inducing necrosis, apoptosis and autophagy in macrophages and foam cells in atherosclerotic plaques, thereby delaying the development of AS. The first-in-man trial has shown that in patients with AS, PTT with silica-gold nanoparticles subjected to intra-vessel NIR irradiation can significantly reduce fibrous tissue and fibro-fatty tissue area and calcification dense in atherosclerotic plaques [6]. MoO<sub>2</sub> nanocluster-based PTT has shown high therapeutic efficacy against AS through the induction of macrophage apoptosis [7]. Further, PDT with nanoparticles encapsulating chlorin e6 was found to attenuate the progression of AS by inducing macrophage apoptosis through the mitochondrial caspase pathway [8]. Additionally, sequential PTT + PDT with chitosan-coated carbon nanocages loaded with chlorin e6 and dextran sulfate was found to target activated macrophages, reduce pro-inflammatory cytokine levels, and inhibit the proliferation and migration of smooth muscle cells [9]. These studies make us believe that nanoparticles-based phototherapy in AS has a practical prospect in clinic, and encourage us to explore safer and more effective photo-therapeutic strategy for AS.

To date, phototherapy for atherosclerotic plaques has largely focused on the regulation of lipid metabolism via inducing cell apoptosis or autophagy. However, high thermal exposure could cause irreversible damage to tissues and vessels. Furthermore, although controlled levels of apoptosis can delay the formation of atherosclerotic plaques, while cell apoptosis itself is an independent risk factor for AS. Excessive apoptosis can enlarge the necrotic core, induce plaque destabilization and ultimately promote acute cardiovascular events [10,11]. Given the challenges in controlling cells apoptosis levels during treatment, novel AS treatment strategy is needed to reduce lipid accumulation, stabilize vulnerable plaques, and avoid plaque cells apoptosis. Heat shock proteins (HSPs), a group of heat-responsive stress proteins, can prevent cell death and apoptosis after exposure to heat [12–15]. Our previous study showed that HSPs in cancer cells can be activated by mild PTT below 45 °C [16]. More importantly, adenovirus-infection induced high expression of wild-type HSP27 has been reported to play key role in lipid metabolism and cholesterol efflux of macrophage-derived foam cells [17]. While it is still not reported that PTT could induce HSP27 expression in foam cells. Consequently, it inspired us that HSP27 might be activated in foam cells under mild PTT and serve as an effective and safe phototherapeutic target for lipid regulation in AS.

In the present study, we verified the effects of mild phototherapy-based HSP activation on lipid metabolism and apoptosis in foam cells. To this end, we designed nanoprobes that allow simultaneous PTT and PDT functions under a single NIR laser excitation. Our previous studies have demonstrated that as a PTT agent, black TiO<sub>2</sub> (bTiO<sub>2</sub>) nanoparticles have high chemical stability, good biocompatibility as well as high photothermal conversion efficiency in the NIR region [18–20]. Herein, we modified bTiO<sub>2</sub> nanoparticles with hyaluronan (HA), and then loaded these modified nanoparticles with the photosensitizer porphine to prepared PTT-PDT bifunctional nanoprobes (bTiO<sub>2</sub>-HA-p). Meanwhile, single PDT and PTT functional nanoprobes were also prepared using HA-modified white TiO<sub>2</sub> (wTiO<sub>2</sub>) nanoparticles loaded with porphine and HA-modified bTiO<sub>2</sub> nanoparticles, respectively. Our findings indicated that bTiO<sub>2</sub> nanoparticles could increase the local temperature to relatively mild levels (44.5 °C) after NIR irradiation. Mild-temperature PTT could prevent excessive cell apoptosis or necrosis and promote ABCA1-dependent cholesterol efflux by activating HSP27

expression, while PDT caused obvious cell death. Furthermore, mild PTT could significantly downregulate SREBP2 triggered biosynthesis and LDLR mediated excess uptake of lipid, upregulate ABCA1-activated cholesterol efflux and therefore reduce intracellular lipid deposition by 5%. In contrast, PDT only decreased intracellular lipid storage by 3%. Interestingly, NIR irradiation of the bTiO<sub>2</sub>-HA-p nanoprobes, which allowed synergetic mild PTT and PDT, activated the SREBP2/LDLR and ABCA1 pathways, thereby attenuating as high as 12.8% of intracellular lipids' accumulation and the formation of macrophage-derived foam cells.

## 2. Materials and methods

### 2.1. Materials

TiO<sub>2</sub> nanoparticles were purchased from Shanghai Musen Industrial Corporation Ltd. Amine-PEG-carboxylic acid (NH<sub>2</sub>-PEG-COOH) and Hyaluronan (HA) (66–99 kDa) were purchased from Xi'an ruixi Biological Technology Co Ltd. 4,4',4'',4'''-(Porphine-5,10,15,20-tetrayl) tetrakis (benzoic acid) (97%) and 1,3-diphenylisobenzofuran (DPBF) were purchased from Aladdin Industrial Inc (Shanghai, China). Dulbecco's modified eagle's medium (DMEM) medium was purchased from GE Healthcare HyClone (LA, USA). Penicillin–streptomycin solution and fetal bovine serum (FBS) were purchased from Gibco (Grand Island, USA). Oxidized low density lipoprotein (ox-LDL) was purchased from AngYuBio (Shanghai, China). Cell Counting Kit-8 (CCK-8) assays was purchased from Beyotime institute of biotechnology (Beijing, China). Ultrapure water (18.2 MΩ cm) was purified by a Millipore Milli-Q system and was used in the following experiments. All other reagents were of analytical grade and used as received.

### 2.2. Synthesis of bTiO<sub>2</sub>-PEG-p, bTiO<sub>2</sub>-HA-p and wTiO<sub>2</sub>-HA-p nanoprobes

#### 2.2.1. bTiO<sub>2</sub>-HA and bTiO<sub>2</sub>-HA-p nanoprobes

First, 50 mg of bTiO<sub>2</sub> were dispersed in 100 mL of ultrapure water and treated with ultrasonic wave for 30 min to allow completely disperse. HA was used to enhance the ability of nanoprobes to target macrophages. 150 mg of HA was dissolved in 10 mL of ultrapure water by ultrasonic for 30 min. Then, dropping HA solution into the bTiO<sub>2</sub> solution. After stirring for 12 h at room temperature, the bTiO<sub>2</sub>-HA nanoprobes were centrifuged at 12,000 rpm for 15 min, washed three times by using ultrapure water and dispersed in 10 mL ultrapure water. After that, 4 mg of the photosensitizer porphine was dissolved in 20 mL ethanol and dropped into bTiO<sub>2</sub>-HA solution under magnetic stirring for 16 h at room temperature. The bTiO<sub>2</sub>-HA-p nanoprobes were obtained by centrifuging at 12,000 rpm three times for 15 min and dispersed into ultrapure water.

#### 2.2.2. wTiO<sub>2</sub>-HA-p nanoprobes

50 mg of white TiO<sub>2</sub> were dispersed in 100 mL of ultrapure water and treated with ultrasonic wave for 30 min. Dropping HA solution into the wTiO<sub>2</sub> solution and stirring for 12 h. Then centrifuged the wTiO<sub>2</sub>-HA solution at 12,000 rpm for 15 min and washed three times. Porphine solution was dropped into wTiO<sub>2</sub>-HA solution under magnetic stirring for 16 h. The wTiO<sub>2</sub>-HA-p nanoprobes were obtained by centrifuging at 12,000 rpm three times for 15 min and dispersed into ultrapure water.

#### 2.2.3. bTiO<sub>2</sub>-PEG-p nanoprobes

NH<sub>2</sub>-PEG-COOH was used to modify the bTiO<sub>2</sub> nanoparticles to improve the dispersity and stability. 100 mg of NH<sub>2</sub>-PEG-COOH was added into 5 mL of ultrapure water and dropped into bTiO<sub>2</sub> solution. Stirring for 12 h at room temperature, the bTiO<sub>2</sub>-PEG nanoprobes were centrifuged at 12,000 rpm for 15 min, washed three times and dispersed in 10 mL ultrapure water. Porphine solution was dropped into bTiO<sub>2</sub>-PEG solution under magnetic stirring for 16 h. The bTiO<sub>2</sub>-PEG-p nanoprobes were obtained by centrifuging at 12,000 rpm three times for

15 min and dispersed into ultrapure water.

### 2.3. Porphine loading rate

Calibration curves of porphine vary from 1 to 6  $\mu\text{g mL}^{-1}$  were used for the concentration calculation. And based on UV–vis absorptions of porphine, the amount of porphine which removed by centrifugation were then calculated, and loaded rate of porphine on the surface of bTiO<sub>2</sub>-PEG, bTiO<sub>2</sub>-HA and wTiO<sub>2</sub>-HA were calculated.

$$\text{Porphine loading (\%)} = \frac{\text{Total mass of porphine in nanoprobe}}{\text{Total mass of nanoprobe}} \times 100\%$$

### 2.4. Characterization of nanoprobe

The concentration of Ti element was measured by inductively coupled plasma optical emission spectrometry (ICP-OES) (Optima 2100, PerkinElmer). Mean size and zeta potential of bTiO<sub>2</sub>-PEG-p, bTiO<sub>2</sub>-HA-p and wTiO<sub>2</sub>-HA-p nanoprobe were performed by Particle Size-Zeta Potential Analyzer (Nano ZS, Malvern Instruments Ltd, England). The morphology of nanoprobe was analyzed by transmission electron microscopy (TEM, Tecnai F20, Thermo Fisher Scientific, USA). Ultraviolet visible (UV–vis) absorption spectra were determined by a UV–visible spectrophotometer (T10CS, Persee General Equipment Co., Ltd, China). Fourier transform infrared (FTIR) spectrum was obtained from a Nicolet 6700 FTIR spectrometer (Thermo Scientific, USA) in the range of 400–4000  $\text{cm}^{-1}$ .

### 2.5. Photothermal performance of nanoprobe

1.0 mL of bTiO<sub>2</sub>-PEG-p, bTiO<sub>2</sub>-HA-p and wTiO<sub>2</sub>-HA-p aqueous solution were added into a disposable dish respectively, and then the solution was irradiated by 808 nm laser under different conditions. (1) bTiO<sub>2</sub>, bTiO<sub>2</sub>-HA, bTiO<sub>2</sub>-HA-p and wTiO<sub>2</sub>-HA-p aqueous solution with different concentrations (0, 75, 100, and 150  $\mu\text{g mL}^{-1}$ ) was irradiated for 15 min at 1.0  $\text{W cm}^{-2}$  (2) bTiO<sub>2</sub>-HA-p aqueous solution (100  $\mu\text{g mL}^{-1}$ ) was irradiated under different power density (0.5, 0.75, and 1.0  $\text{W cm}^{-2}$ ) for 15 min. Temperatures were recorded per 30 s. The temperature changes and thermographic images were performed by photothermal imaging system.

### 2.6. Photodynamic effect of nanoparticle

1,3-diphenylisobenzofuran (DPBF) was used as a chemical probe to detect singlet oxygen. 100  $\mu\text{g mL}^{-1}$  of bTiO<sub>2</sub>, porphine, bTiO<sub>2</sub>-PEG-p or bTiO<sub>2</sub>-HA-p nanoprobe were dispersed in ethanol containing 20  $\mu\text{L}$  of DPBF (25  $\mu\text{g mL}^{-1}$ ). 1 mL of these dispersions were irradiated by 808 nm NIR laser at 1  $\text{W cm}^{-2}$  for 10 min. Using fluorescence spectral to analyze the fluorescence intensity every single minute ( $\lambda_{\text{ex}} = 411 \text{ nm}$ ).

### 2.7. Cell culture and foam cell formation

The RAW 264.7 cells were obtained from the Cell Bank of the Chinese Academy of Sciences (Shanghai, China). Cells were cultured in DMEM medium with 10% FBS and 1% antibiotics (100 U  $\text{mL}^{-1}$  penicillin-streptomycin solution) and incubated in a 5% CO<sub>2</sub> air humidified incubator at 37 °C. For the experiments, RAW 264.7 cells were seeded at a density of  $1 \times 10^5$  cells/well in 96-well plates and cultured overnight, then stimulated with 50  $\mu\text{g mL}^{-1}$  ox-LDL in serum-free DMEM medium for 48 h to induce foam cells formation.

### 2.8. Cell viability assay

The cell viability of RAW 264.7 cells were detected by CCK-8 assay according to the manufacturer's protocol. Briefly, RAW264.7 cells were seeded in 96-well plates ( $2 \times 10^4$  cells/well) and incubated with

complete DMEM medium at a 37 °C and 5% CO<sub>2</sub> atmosphere for 24 h. Then, 100  $\mu\text{L}$  of diverse concentrations (0, 25, 50, 75 and 100  $\mu\text{g mL}^{-1}$ ) of bTiO<sub>2</sub>-HA, bTiO<sub>2</sub>-HA-p and wTiO<sub>2</sub>-HA-p nanoprobe were added into each well respectively. After being incubated for 24 h, cells were washed with PBS for three times and cultured with 100  $\mu\text{L}$  of DMEM medium containing 10  $\mu\text{L}$  CCK-8 solution for another 2 h. The absorbance was performed by a microplate reader (iMark 168–1130, Bio-rad, USA) at 450 nm wavelength. The treated cell viability was calculated as a percentage of the absorbance to control one. Each test was repeated three times.

### 2.9. Investigation of intracellular ROS

The intracellular ROS generation was detected by a fluorescent probe 2', 7'-dichlorofluorescein diacetate (DCFH-DA). Briefly, RAW 264.7 cells were seeded in 24-well plates at  $1 \times 10^5$  cells/well and incubated for 24 h. After that, cells were treated with 100  $\mu\text{L}$  of bTiO<sub>2</sub>-HA, bTiO<sub>2</sub>-HA-p and wTiO<sub>2</sub>-HA-p (75  $\mu\text{g mL}^{-1}$ ) respectively and cultured for 4 h. The positive control group were prepared with 100  $\mu\text{L}$  of 50 mM H<sub>2</sub>O<sub>2</sub> for 20 min. After that, the cells were washed with PBS for three times and treated with DCFH-DA solution for 20 min at 37 °C in the dark. The cells were washed with DMEM for three times and then exposed to 808 nm laser for different times. The fluorescence was performed by a fluorescent microscope (Leica DMI3000).

### 2.10. Cellular uptake

Cellular uptake of bTiO<sub>2</sub>-PEG-p, bTiO<sub>2</sub>-HA-p and wTiO<sub>2</sub>-HA-p nanoprobe in RAW264.7 cells were observed by confocal laser scanning microscope (CLSM), flow cytometry and ICP.

#### 2.10.1. Cellular uptake observed by CLSM

Cells were seeded in CLSM dishes at  $3 \times 10^4$  cells/well and incubated with complete DMEM medium for 24 h. Then, cells were incubated with fresh medium, bTiO<sub>2</sub>-PEG-p, bTiO<sub>2</sub>-HA-p or wTiO<sub>2</sub>-HA-p nanoprobe (Ti concentrations: 75  $\mu\text{g mL}^{-1}$ ) for another 4 h. Next, cells were washed with PBS for three times, and were stained with Hoechst and FITC for 30 min at 4 °C in the dark.

#### 2.10.2. Cellular uptake observed by flow cytometry

Cells were seeded in 12-well plates at  $2 \times 10^5$  cells/well and incubated with complete DMEM medium for 24 h. After that, the culture medium was replaced by fresh medium, bTiO<sub>2</sub>-PEG-p or bTiO<sub>2</sub>-HA-p nanoprobe (Ti concentrations: 75  $\mu\text{g mL}^{-1}$ ) and incubated for 4 h. Then cells were collected to detect the fluorescence intensity of porphine using flow cytometry.

#### 2.10.3. Cellular uptake observed by ICP

Cells were seeded in 6-well plates at  $3 \times 10^5$  cells/well and incubated with complete DMEM medium for 24 h. After that, the culture medium was replaced by fresh medium, bTiO<sub>2</sub>-PEG-p, bTiO<sub>2</sub>-HA-p or wTiO<sub>2</sub>-HA-p nanoprobe (Ti concentrations: 75  $\mu\text{g mL}^{-1}$ ) and incubated for 2, 4, 8, 12 h, respectively. After being digested by acid solution, cells were collected to investigate the concentration of Ti element by ICP.

### 2.11. Mild phototherapy in vitro

Foam cells were seeded in 6-well plates at  $3 \times 10^5$  cells/well and incubated with complete DMEM medium for 24 h before treatment. After that, cells were incubated with fresh medium, bTiO<sub>2</sub>-PEG-p, bTiO<sub>2</sub>-HA-p and wTiO<sub>2</sub>-HA-p nanoprobe (TiO<sub>2</sub> concentrations: 75  $\mu\text{g mL}^{-1}$ ) for another 4 h, respectively. Then, cells were washed with PBS for three times and exposed to 808 nm laser at 1  $\text{W cm}^{-2}$  for 10 min.

#### 2.11.1. Live and dead cell assay

After the treatment for 8 h, cells were stained with calcein-AM and

propidium iodide (PI) solution for 15 min. Live cells were stained in green and dead cells were in red.

### 2.11.2. Foam cell formation assay

After the treatment for 8 h, cells were washed with PBS for 3 times, fixed with 4% paraformaldehyde for 20 min, washed with 60% isopropanol and finally stained with Oil Red O for 30 min. Using optical microscope to photograph cells, and the percentage of lipid droplets area to total cells were measured using an en-face method by ImageJ.

### 2.12. Quantitative real-time polymerase chain reaction (qRT-PCR)

Total RNA was extracted by Trizol reagent and purified from macrophage derived foam cells (Invitrogen, Carlsbad, CA, USA). Complementary DNA (cDNA) was synthesized using the HiFiScript first-strand cDNA synthesis kit (ComWin Biotech, Beijing, China) according to the manufacturer's instructions. PCR amplification was accomplished using  $1 \times$  FastStart Essential DNA Green Master (Roche, Mannheim, Germany) with a LightCycler 480 II instrument (Roche, Switzerland). The primer sequences used included (forward and reverse): HSP27 rRNA, 5'-TGCTTCACCCGAAATACAC-3' and 5'-CTCGAAAGTAACCGGAATGG-3'; SREBP2 rRNA, 5'-TGGCGGATGAGCTGACTCT-3' and 5'-CAAATCAGGGAAGTCTCCAC-3'; LDLR rRNA, 5'-TGATGGACAGGCCCTAACT-3' and 5'-CTGCCTCTTGAACAGTGTCC-3'; ABCA1 rRNA, 5'-GCTCTCAGGTGGGATGCAG-3' and 5'-GGCTCGTCCAGAAATGACAAC-3'; GAPDH rRNA, 5'-CTCGTCCCGTAGACAAAATGGT-3' and 5'-GAGGTCAATGAAGGGGTCGTT-3'. Data were normalized to GAPDH rRNA and the dosage of the target fragments was calculated using the  $2^{-\Delta\Delta CT}$  method. Sequences were confirmed using NCBI BLAST software.

### 2.13. Western blotting

After the treatments, cells were washed by ice-cold PBS for twice and scraped in RIPA lysis buffer for 20 min at 4 °C to extract total proteins. The protein concentrations were quantified by the bicinchoninic acid (BCA) kit (Beyotime Biotechnology, Beijing, China). Quantified protein samples were separated on sodium dodecyl sulfate polyacrylamide gel electrophoresis (SDS-PAGE) and transferred to a 0.45  $\mu$ m polyvinylidene fluoride membranes (Merck Millipore, Darmstadt, Germany). Using 0.05% TBST to wash the membranes and blocking with 0.05% TBST containing 5% non-fat milk at room temperature for 1 h. Then, the membranes were incubated with 0.05% TBST containing the primary antibody overnight at 4 °C, and followed by the horseradish peroxidase-conjugated secondary antibody for 1 h at room temperature. After washed with 0.05% TBST for three times, the immune complexes were detected by enhanced chemiluminescence kit and the protein bands were visualized by a chemiluminescence imaging system (ChemiScope 6200 Touch, CLiNX, Shanghai, China).

Antibody sources were as follows: anti-LDL Receptor rabbit antibody (1:500 dilution, ab52818), anti-SREBP2 rabbit antibody (1:500 dilution, ab30682), anti-beta Actin antibody (1:1000 dilution, ab8227, Abcam, Cambridge, UK); anti-HSP27 (1:500 dilution, AF0183, Beyotime Biotechnology, Beijing, China); anti-ABCA1 (1:500 dilution, AF6114, Beyotime Biotechnology, Beijing, China).

### 2.14. Statistical analysis

Data were presented as mean  $\pm$  standard deviation (SD). Statistical analysis was conducted by GraphPad Prism 7 (GraphPad Software, San Diego, CA, USA) using the one-way ANOVA test for experiments consisting of more than two groups, and with a two-tailed, unpaired *t*-test in experiments with two groups. *p* < 0.05 was assessed as statistical significance.

## 3. Results and discussion

### 3.1. Preparation and characterization of various nanoparticles

The process of nanoprobe synthesis is illustrated in Fig. 1. In order to verify the differential effects of PTT, PDT, and synergistic PTT + PDT on foam cells, bTiO<sub>2</sub>-HA, wTiO<sub>2</sub>-HA-p, and bTiO<sub>2</sub>-HA-p nanoprobe were prepared. Among these, bTiO<sub>2</sub>-HA possessed only photothermal properties, wTiO<sub>2</sub>-HA-p possessed only photodynamic properties, and bTiO<sub>2</sub>-HA-p showed both photothermal and photodynamic effects under 808 nm NIR irradiation. The morphology of the different bTiO<sub>2</sub> nanoparticles was examined using TEM. As illustrated in Fig. 2A, bare bTiO<sub>2</sub> nanoparticles showed poor dispersion and a high tendency to agglomerate. NH<sub>2</sub>-PEG-COOH and HA contain hydrophilic groups, such as carboxyl and hydroxyl. After coating bTiO<sub>2</sub> nanoparticles with NH<sub>2</sub>-PEG-COOH or HA, the formed hydrophilic protective layers on surface of nanoprobe could improve steric stabilization, biocompatibility as well as blood circulation half-life [21]. And the results in Fig. 2A and Fig. S1 showed that dispersity and stability of the nanoprobe were improved after modified with NH<sub>2</sub>-PEG-COOH or HA. Dynamic light scattering (DLS) experiments indicated that the average size of bTiO<sub>2</sub>, bTiO<sub>2</sub>-HA, and bTiO<sub>2</sub>-HA-p was 95 nm, 191  $\pm$  1.8 nm, and 211  $\pm$  2 nm, respectively (Fig. 2B). All these nanoprobe also showed significant negative zeta-potential values in ultrapure water (Fig. 2C). In addition, the UV-vis absorbance spectra of bTiO<sub>2</sub>, bTiO<sub>2</sub>-HA-p (Fig. 2D), bTiO<sub>2</sub>-PEG-p, and wTiO<sub>2</sub>-HA-p nanoprobe (Fig. S3) showed an absorption peak characteristic of porphine at 417 nm, indicating that porphine had been successfully attached to the surface of the nanoprobe. The FTIR spectra of the different nanoparticles are displayed in Fig. 2E. The peak at 600–500 cm<sup>-1</sup> was attributed to the Ti–O bond. The spectrum of porphine contained many absorption peaks. The peaks at 1604–1300 cm<sup>-1</sup>, 1000 cm<sup>-1</sup>, and 965 cm<sup>-1</sup> were ascribed to the C=N stretching vibration, benzene skeleton vibration, and N–H bond in porphine, respectively. bTiO<sub>2</sub>-HA-p also showed the peaks characteristic of porphine, confirming the successful loading of the photosensitizer porphine onto the surface of the nanoprobe.

### 3.2. Photothermal performance of bTiO<sub>2</sub>-HA-p nanoprobe

To evaluate photothermal performance, bTiO<sub>2</sub>-HA-p nanoprobe were dispersed in pure water at various concentrations ranging from 0 to 150  $\mu$ g mL<sup>-1</sup>. Subsequently, they were irradiated with an 808 nm laser at power densities ranging from 0.5 to 1.0 W cm<sup>-2</sup>. As shown in Fig. 3A–B, bTiO<sub>2</sub>-HA-p nanoprobe displayed a concentration- as well as power density-dependent photothermal performance. Specifically, the temperature of the 100  $\mu$ g mL<sup>-1</sup> bTiO<sub>2</sub>-HA-p dispersion increased rapidly from 25 °C to 46.1 °C within 10 min after continuous irradiation with 808 nm NIR laser at 1 W cm<sup>-2</sup>. In contrast, the temperature of deionized water rose by only 1.4 °C under the same conditions. The temperature also increased with the concentration of the nanoprobe and the duration of NIR irradiation, demonstrating that the bTiO<sub>2</sub>-HA-p nanoprobe are good photothermal agents.

### 3.3. Photodynamic performance of bTiO<sub>2</sub>-HA-p nanoprobe

ROS induce an irreversible decrease in the fluorescence intensity of DPBF. Therefore, DPBF is used for the specific detection of ROS [22]. As shown in Fig. 3C, after pre-incubation with bTiO<sub>2</sub>-HA-p and 10 min of continuous irradiation with an 808 nm NIR laser (1 W cm<sup>-2</sup>), the fluorescence intensity of DPBF decreased by 80%. In contrast, pre-incubation with porphine-free nanoprobe resulted in a marginal decrease only, demonstrating the effective photodynamic properties of bTiO<sub>2</sub>-HA-p nanoprobe.

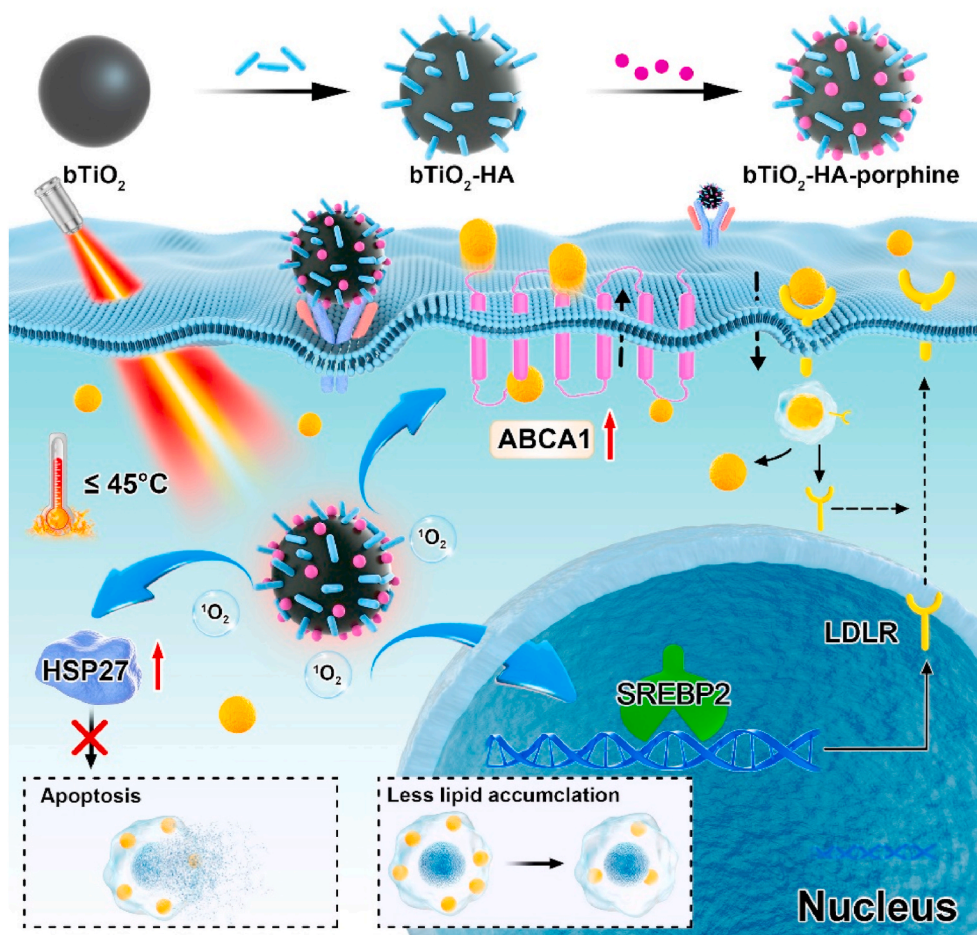


Fig. 1. Schematic illustration of lipid metabolism in foam cells after phototherapy with  $\text{bTiO}_2$ -based nanoprobes irradiated by 808 nm NIR laser.

### 3.4. Cell targeting

To examine foam cells targeting ability of  $\text{bTiO}_2$ -HA-p,  $\text{bTiO}_2$ -PEG-p nanoprobes were used as a negative control. The cellular uptake of both these nanoprobes increased with an increased incubation period, and the concentration of Ti element in  $\text{bTiO}_2$ -HA-p-treated cells was higher than that in  $\text{bTiO}_2$ -PEG-p-treated cells at all time points (Fig. 4A). Meanwhile, although porphyrin fluorescence could be observed in cells treated with both  $\text{bTiO}_2$ -PEG-p and  $\text{bTiO}_2$ -HA-p (Fig. 4B), the intensity was significantly stronger in the  $\text{bTiO}_2$ -HA-p group (93.0) than in the  $\text{bTiO}_2$ -PEG-p group (45.9,  $p < 0.01$ , Fig. 4C). These results demonstrated that HA modification could enhance uptake of nanoprobes in foam cells, which are mainly because macrophages express HA-binding receptors, such as CD44, LYVE-1, RHAMM, TLR4 [23].

Subsequently, the intracellular localization of  $\text{bTiO}_2$ -PEG-p,  $\text{bTiO}_2$ -HA-p, and  $\text{wTiO}_2$ -HA-p in foam cells was also tested using confocal microscopy (Figs. 4D and S6). Bright-field images showed that the uptake of nanoprobes caused no obvious changes in cell morphology. After incubation, the  $\text{bTiO}_2$ -PEG-p,  $\text{bTiO}_2$ -HA-p, and  $\text{wTiO}_2$ -HA-p nanoprobes were phagocytosed by foam cells and became distributed in their cytoplasm. Fluorescence accumulation was highest in the  $\text{bTiO}_2$ -HA-p group, further demonstrating that  $\text{bTiO}_2$ -HA-p nanoprobes can target macrophage-derived foam cells and thereby enhance therapeutic effects.

### 3.5. Analysis of cellular ROS production

To evaluate the potential photodynamic properties of  $\text{bTiO}_2$ -HA,  $\text{bTiO}_2$ -HA-p, and  $\text{wTiO}_2$ -HA-p, the intracellular ROS generation induced by different nanoprobes was tested using DCFH-DA, a  $\text{H}_2\text{O}_2$  indicator

that rapidly generates green fluorescence in the presence of ROS. As shown in the fluorescence images, cells treated with  $\text{H}_2\text{O}_2$  showed strong green fluorescence (Fig. S7). However, cells pre-incubated with  $\text{bTiO}_2$ -HA showed negligible fluorescence, while those pre-incubated with  $\text{bTiO}_2$ -HA-p and  $\text{wTiO}_2$ -HA-p produced significant green fluorescence after irradiation with an 808 nm laser for 10 min (Fig. 5). These findings indicated that  $\text{bTiO}_2$ -HA-p could generate substantial amounts of ROS under NIR irradiation and that the photodynamic activity of  $\text{bTiO}_2$ -HA-p was enhanced after porphine loading.

### 3.6. Phototherapy in foam cells

The toxicity profiles of nanoprobes are crucial determinants of their future use. To test toxicity of nanoprobes, foam cells were incubated with various concentrations of  $\text{bTiO}_2$ -HA,  $\text{bTiO}_2$ -HA-p, and  $\text{wTiO}_2$ -HA-p for 24 h (Fig. 6A). Negligible effects on cell viability were observed, even when the nanoprobes' concentration reached  $100 \mu\text{g mL}^{-1}$ , indicating the good biocompatibility of  $\text{bTiO}_2$ -HA-p. The photothermal curves of *in vitro* phototherapy revealed that treatment with  $75 \mu\text{g mL}^{-1}$  of the nanoprobes and  $1.0 \text{ W cm}^{-2}$  NIR irradiation allowed the treatment temperature to be maintained under  $45^\circ\text{C}$ . After 10 min of irradiation, cell viabilities significantly reduced only in the PDT group ( $\text{wTiO}_2$ -HA-p + Laser, 79.6%,  $p < 0.05$ ), while the cell viabilities in mild PTT or mild PTT + PDT groups remained above 90% (Fig. 6B). To visually observe phototherapy performance, cells were stained with calcein-AM (live, green) and PI (dead, red). Consistent with the cell viability results, PDT group was observed a high number of dead cells (Fig. 6C). Interestingly, although PDT caused evident cell apoptosis or necrosis, most foam cells in mild PTT or mild PTT + PDT group remained viable.

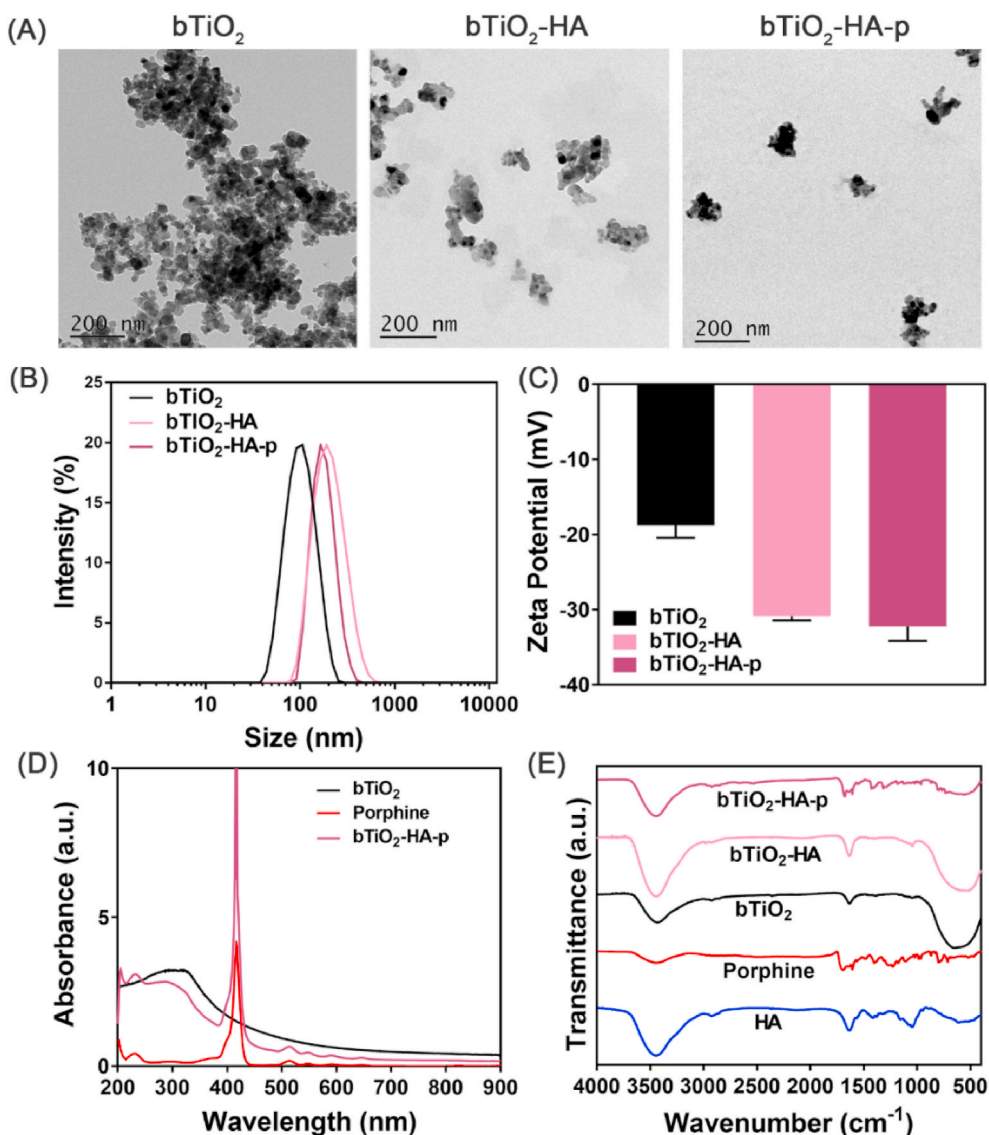


Fig. 2. (A) Transmission electron microscopy images of bTiO<sub>2</sub>, bTiO<sub>2</sub>-HA, and bTiO<sub>2</sub>-HA-p, and the corresponding (B) dynamic light scattering curves, (C) zeta potential, and (D) UV-vis absorbance spectra. (E) Fourier-transform infrared spectra of HA, porphine, bTiO<sub>2</sub>, bTiO<sub>2</sub>-HA, and bTiO<sub>2</sub>-HA-p.

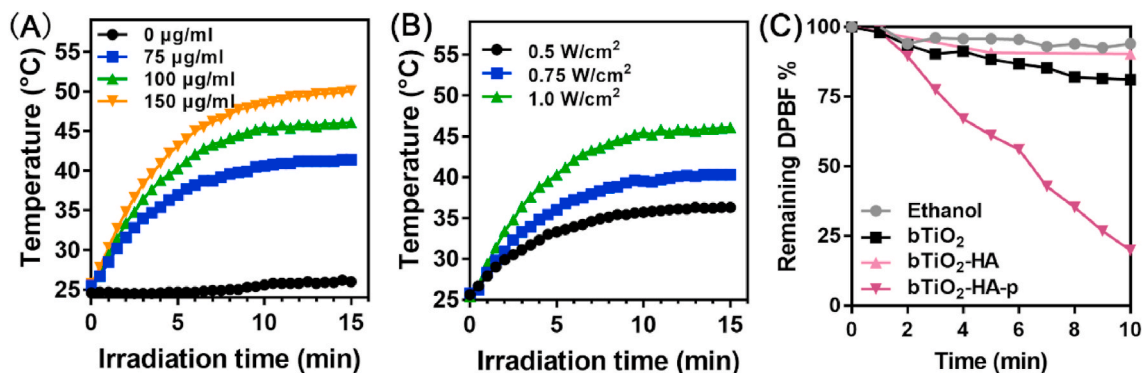


Fig. 3. Temperature evolution curves of bTiO<sub>2</sub>-HA-p dispersion at (A) different concentrations (1 W cm<sup>-2</sup>) and (B) different power densities (100 µg mL<sup>-1</sup>). (C) Time-dependent ROS productions of bTiO<sub>2</sub>, bTiO<sub>2</sub>-HA, and bTiO<sub>2</sub>-HA-p under 808 nm laser irradiation (1 W cm<sup>-2</sup>) evaluated based on the proportion of residual DPBF fluorescence.

To further elucidate these results, we used a photothermal imaging system and performed continuous temperature monitoring of foam cells during 808 nm laser irradiation (Fig. 7A–B). The change in temperature

was negligible in the PDT group, but a mild increase was noted in the PTT + PDT group. Irradiation with 1.0 W cm<sup>-2</sup> of 808 nm laser for 10 min increased the temperature of cells pre-incubated with bTiO<sub>2</sub>-HA-p

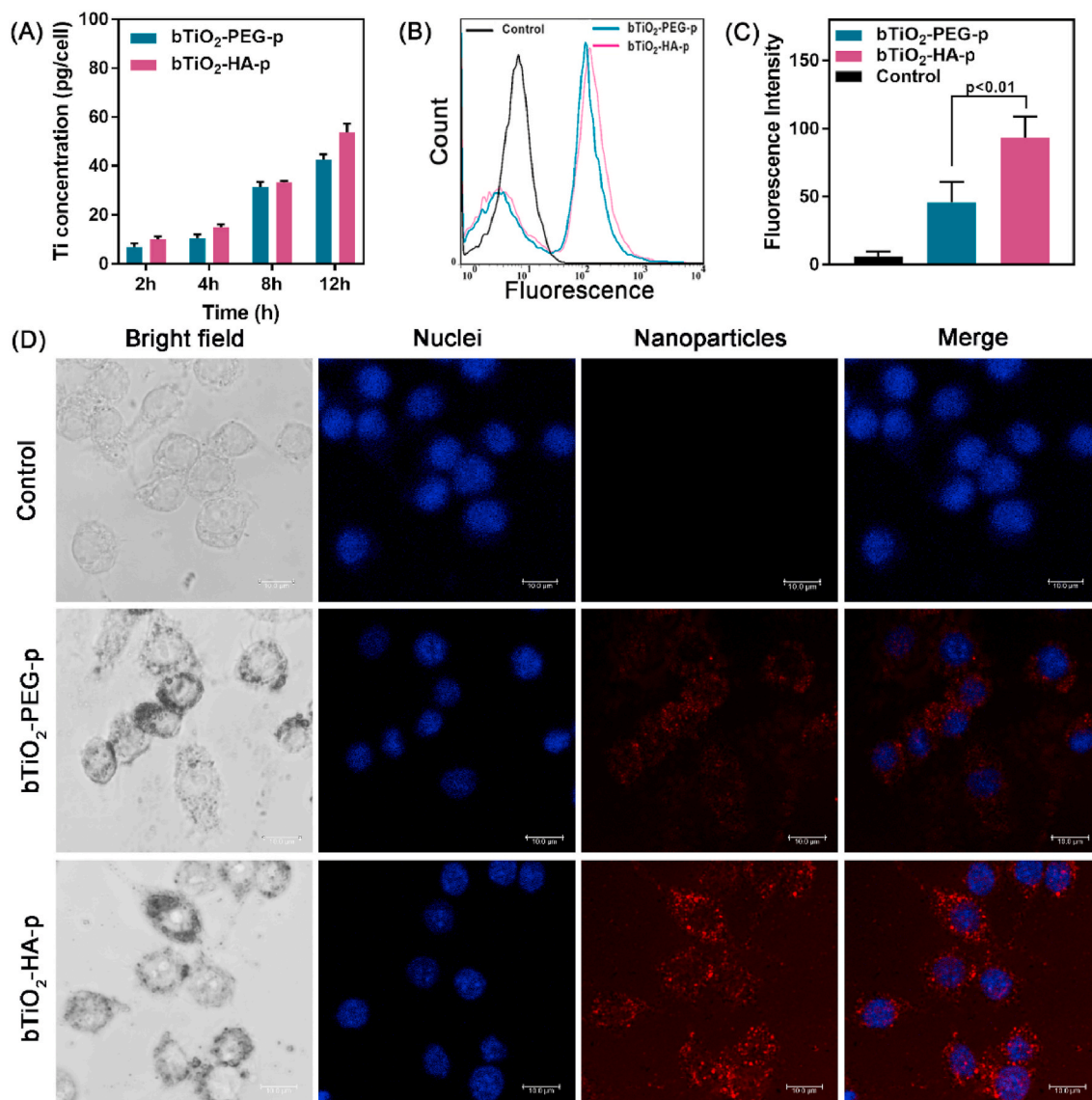


Fig. 4. (A) Uptake of bTiO<sub>2</sub>-PEG-p and bTiO<sub>2</sub>-HA-p by foam cells after different incubation periods. (B) Fluorescence distribution and (C) intensity in foam cells incubated with culture medium, bTiO<sub>2</sub>-PEG-p, or bTiO<sub>2</sub>-HA-p for 4 h. (D) Confocal images of foam cells incubated with or without nanoprobe for 4 h. Scale bar: 10 μm.

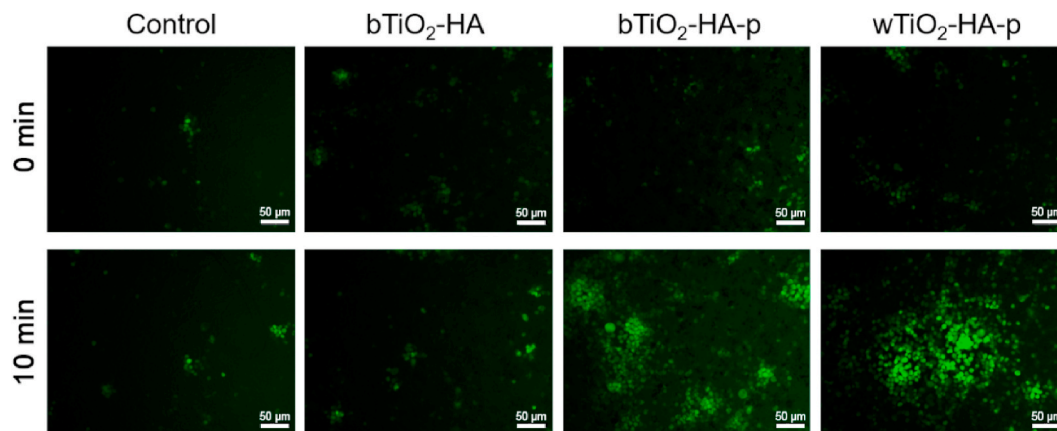


Fig. 5. Fluorescence images indicating the generation of ROS in normal foam cells and foam cells pre-incubated with bTiO<sub>2</sub>-HA, bTiO<sub>2</sub>-HA-p, and wTiO<sub>2</sub>-HA-p after 808 nm laser irradiation (1 W cm<sup>-2</sup>). DCFH-DA was used as an indicator of ROS generation. Scale bar = 50 μm.

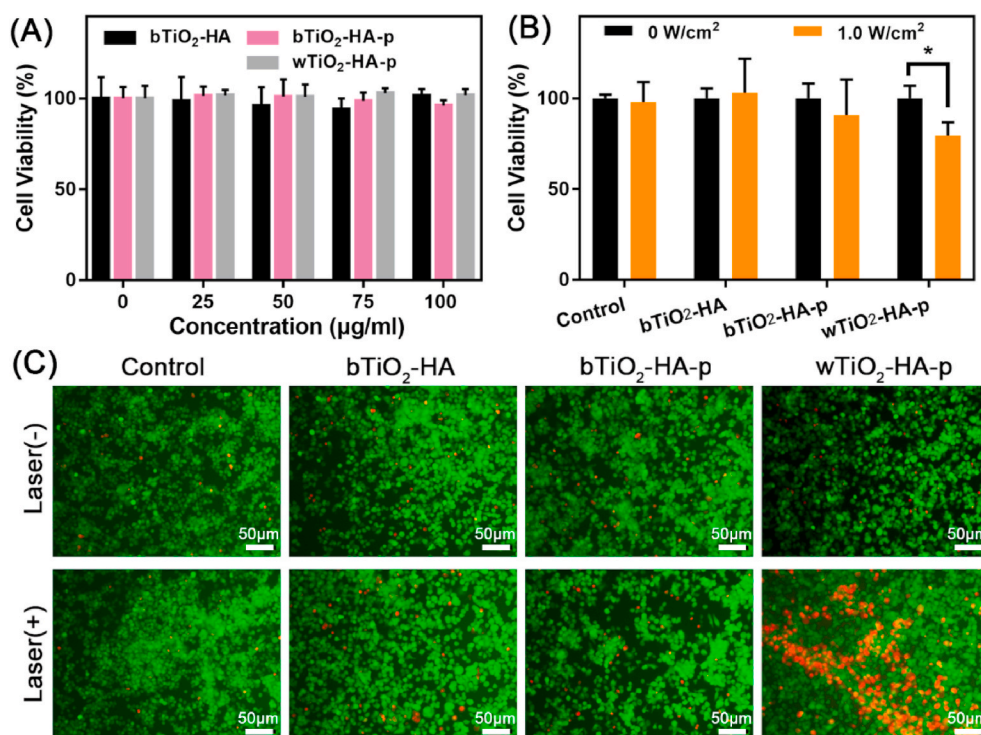


Fig. 6. Cell viabilities of foam cells incubated with (A) various concentrations of bTiO<sub>2</sub>-HA, bTiO<sub>2</sub>-HA-p, and wTiO<sub>2</sub>-HA-p and (B) irradiated with different power densities using 808 nm laser (75 µg mL<sup>-1</sup>, 10 min). \**p* < 0.05. (C) Corresponding fluorescence images of live and dead foam cells. Cells were stained by calcein-AM and PI, green: alive, red: dead. Scale bar = 50 µm. (For interpretation of the references to colour in this figure legend, the reader is referred to the Web version of this article.)

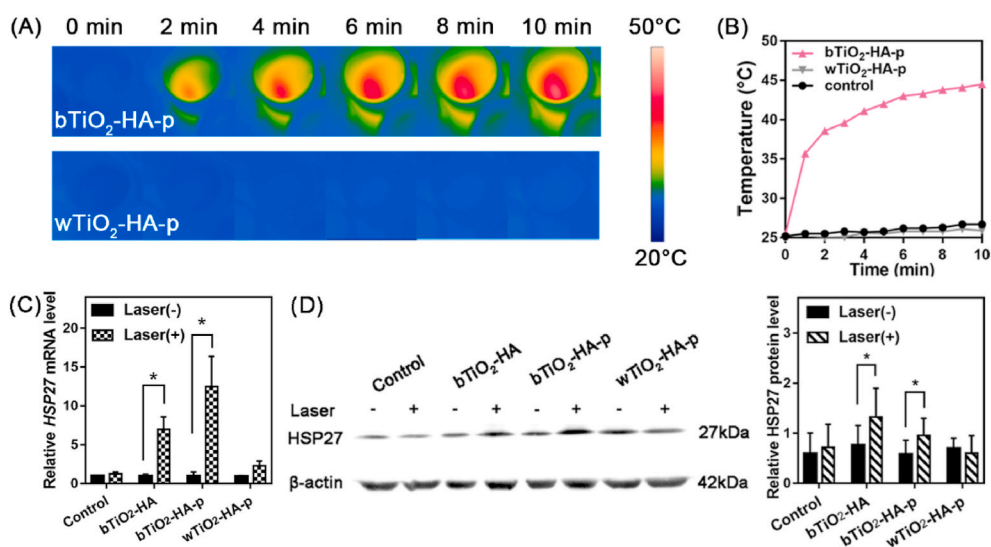


Fig. 7. (A) Infrared thermal images of foam cells pretreated with bTiO<sub>2</sub>-HA-p and wTiO<sub>2</sub>-HA-p (75 µg mL<sup>-1</sup>) and irradiated using an 808 nm laser (1.0 W cm<sup>-2</sup>, 10 min), and (B) corresponding temperature curves. (C) Relative HSP27 mRNA expression in foam cells after different treatments. (D) Western blot images and quantified HSP27 protein levels in foam cells after different treatments. β-actin was used as a loading control. \**p* < 0.05.

from 25.5 °C to 44.5 °C. It has been widely reported that during mild-temperature PTT for cancer, cells upregulate HSPs in order to protect themselves against hyperthermia [24,25]. HSP27, a member of the HSP family, is a novel anti-atherosclerotic biomarker and inhibits cell apoptosis via both extrinsic and intrinsic pathways [13–15,26]. Here, to explore the different effects observed in foam cells after the various forms of phototherapy, we examined changes in both gene and protein expression in treated cells. As shown in Fig. 7C, the mRNA expression of HSP27 was obviously increased in the mild PTT alone (7.3-fold, *p* < 0.05) and mild PTT + PDT (12.5-fold, *p* < 0.05) groups, although the PDT alone (2.4-fold) and control (1.3-fold) groups did not show any significant difference. This demonstrated that HSP27 mRNA expression

could indeed be triggered by mild-temperature PTT in foam cells. Meanwhile, Western blot assays were also used to evaluate the protein levels of HSP27 in foam cells after different treatments (Fig. 7D). Consistent with gene expression findings, the expression of the HSP27 protein increased by approximately 1.7-fold in mild-temperature PTT group and 1.6-fold in mild PTT + PDT group (*p* < 0.05) after laser irradiation, respectively. In contrast, the PDT alone and control groups showed a negligible difference. It was the protective effect of HSP27 that made the cell viability in mild PTT + PDT group above 90%, even in the presence of ROS. Therefore, our results suggested that mild-temperature phototherapy with bTiO<sub>2</sub>-HA and bTiO<sub>2</sub>-HA-p nanoprobe could effectively upregulate HSP27 expression, remarkably enhance

thermo-resistance in foam cells, and thereby inhibit cell apoptosis or necrosis.

Several studies have examined the mechanisms via which phototherapy inhibits the development of AS, and cellular apoptosis pathways have primarily been implicated in this process. Wang et al. found that MoO<sub>2</sub> nanocluster-based PTT leads to macrophage elimination via the Bcl-2/Bax/Caspase-3 pathway-mediated induction of cell apoptosis [7]. Single-walled carbon nanotubes, another efficient photothermal ablation agent, were also found to upregulate Caspase-3 and induce apoptosis and thereby ablate vascular macrophages [27]. Pyropheophorbide- $\alpha$  methyl ester-mediated PDT has been shown to induce apoptosis in RAW264.7 cells via the activation of the mitochondrial caspase pathway [28]. However, the excessive apoptosis of plaque cells is an independent risk factor for AS and contributes to impaired phagocytic clearance of macrophages, resulting in a pro-inflammatory response and secondary necrosis. Such excessive apoptosis thus increases the instability of atherosclerotic plaques and causes thrombosis, leading to acute cardiovascular events [4,29,30]. Additionally, moderating cell apoptosis during treatment is challenging. In this study, we found that mild phototherapy with bTiO<sub>2</sub>-HA-p nanoprobes does not cause significant cell apoptosis. To investigate the lipid regulatory effects of mild phototherapy with the nanoprobes, we examined the intracellular lipid burden of foam cells incubated with bTiO<sub>2</sub>-HA, bTiO<sub>2</sub>-HA-p, and wTiO<sub>2</sub>-HA-p in the presence or absence of 808 nm laser irradiation. As shown in Fig. 8 and Fig. S8, oil red O staining indicated that the cells were full of lipid droplets after treatment with ox-LDL for 48 h. After 808 nm laser irradiation, lipid deposition in the mild PTT group decreased from 22.5% to 17.5% ( $p < 0.05$ ), and in the mild PTT + PDT group, these values showed a remarkable reduction from 25.3% to 12.5% ( $p < 0.01$ ). In the PDT alone group, only a slight reduction in lipid deposition was observed (from 24.5% to 21.5%,  $p > 0.05$ ). Therefore, the results indicated that mild PTT + PDT causes synergistic effects on the regulation of lipid homeostasis, without inducing significant cell apoptosis or necrosis.

Intracellular cholesterol homeostasis is determined by the balance between cholesterol biosynthesis, uptake and cholesterol efflux. These processes are tightly controlled by multiple transcriptional and post-translational regulatory systems. Sterol regulatory element-binding

protein 2 (SREBP2) plays an important role in the lipid biosynthesis pathway. In general, when the intracellular cholesterol levels are low, the SREBP2 pathway is activated. This pathway selectively upregulates target genes, such as low-density lipoprotein receptor (LDLR), resulting in the biosynthesis of cholesterol [31]. In contrast, in the presence of excess cholesterol levels, SREBP2 cleavage is inhibited, and consequently, the transcription of target genes and cholesterol biosynthesis are both downregulated [31]. As shown in Fig. 9A–B, *SREBP2* mRNA expression was significantly lower in the mild PTT + PDT group than in the corresponding non-irradiated group. Both the mild PTT and PDT alone groups showed marginally lower *SREBP2* mRNA expression than the corresponding non-irradiated groups. In line with this, *SREBP2* protein levels decreased by about 1.76-fold after irradiation in the mild PTT + PDT group, and slight downregulation was observed in the mild PTT group (Fig. 9B). These data indicated that bTiO<sub>2</sub>-triggered mild PTT and mild PTT + PDT could attenuate lipid biosynthesis by inhibiting the *SREBP2* pathway.

LDLR is responsible for the cellular uptake of lipids, and this gene is also a transcriptional target of *SREBP2*. LDLR is expressed on the surface of cell membranes and captures free LDL through its extracellular ligand binding domain, thus endocytosing LDL through vesicles. Subsequently, a portion of the LDLR protein dissociates from the bound LDL and returns to the cell surface, ready for further rounds of LDL endocytosis. The cholesteryl esters carried by LDL are finally hydrolyzed into cholesterol inside cells by lipase. Therefore, factors that affect the biosynthesis of LDLR could also affect cellular lipid uptake. In our study, *LDLR* mRNA expression was significantly downregulated in the mild PTT + PDT group after laser irradiation (Fig. 9C). A decreasing trend was also noted in the mild PTT and PDT alone groups. Moreover, LDLR protein expression was reduced in the mild PTT and mild PTT + PDT groups after laser irradiation. These results together suggested that bTiO<sub>2</sub>-triggered mild PTT and mild PTT + PDT can reduce lipid uptake by inhibiting the expression of *LDLR* mRNA.

In addition to cholesterol uptake and biosynthesis, cholesterol efflux also has a critical role in intracellular cholesterol homeostasis. This process is governed by ATP-binding cassette transporters, one of which is ATP-binding cassette transporter A1 (ABCA1). ABCA1 promotes the removal of cholesterol load and mediates cholesterol transport from

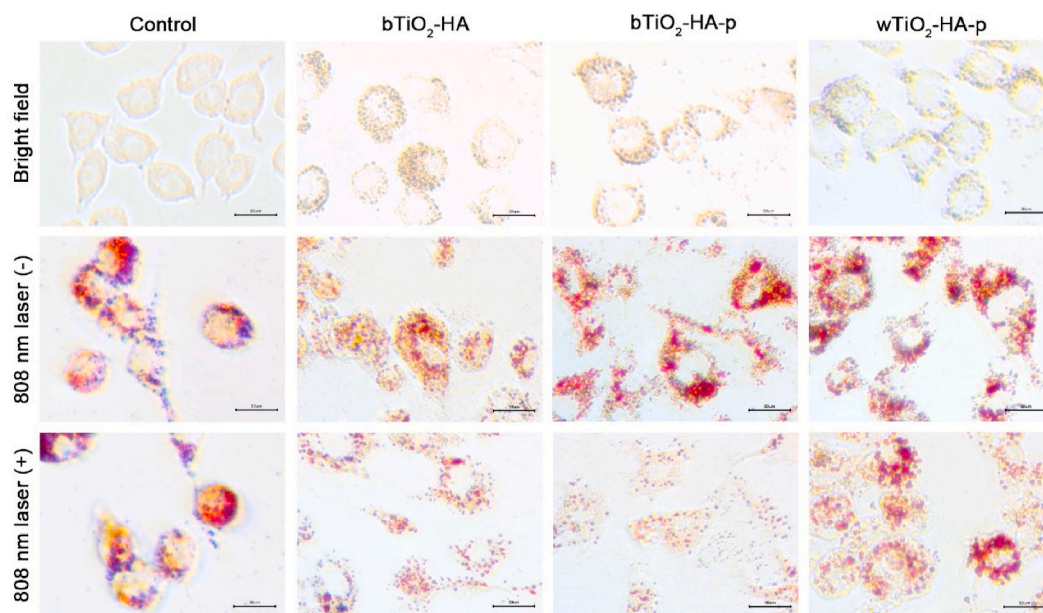


**Fig. 8.** Effects of mild phototherapy on the intracellular lipid burden. Representative images of oil red O staining of lipid deposits in foam cells in the control, bTiO<sub>2</sub>-HA, bTiO<sub>2</sub>-HA-p, and wTiO<sub>2</sub>-HA-p groups with and without 808 nm laser irradiation (1.0 W cm<sup>-2</sup>, 10 min). Scale bar = 50  $\mu$ m. (For interpretation of the references to colour in this figure legend, the reader is referred to the Web version of this article.)

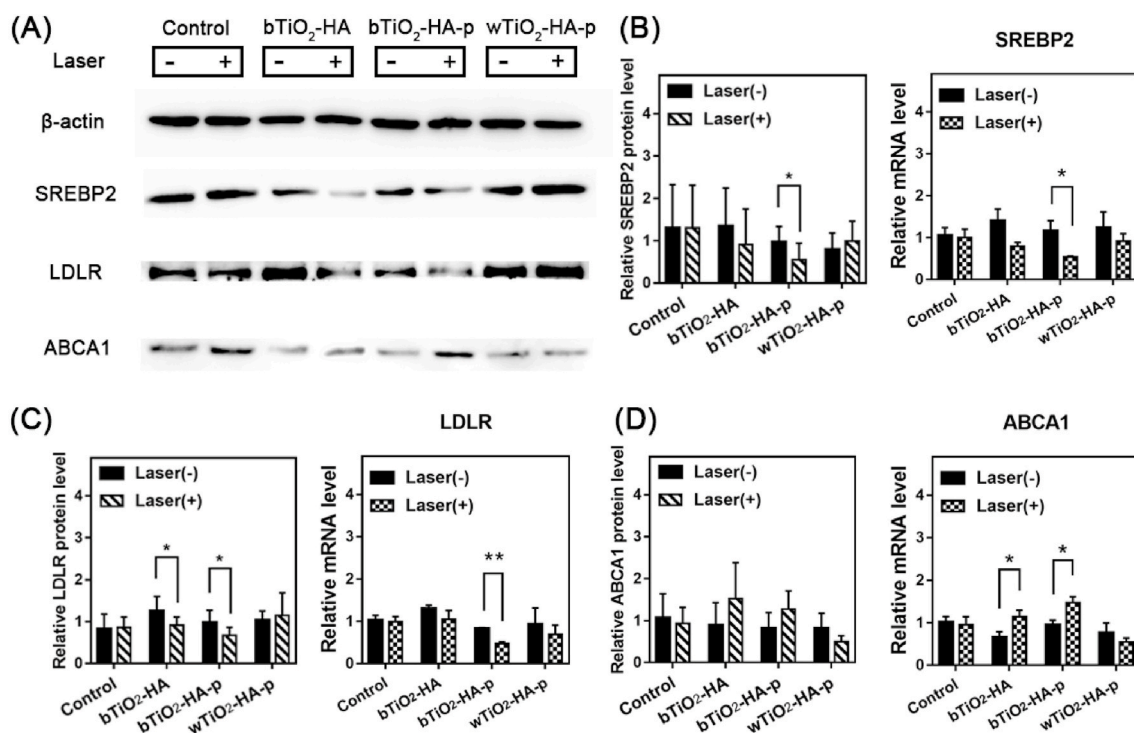


**Fig. 9.** Examination of the mechanism underlying the effects of mild phototherapy on lipid metabolism. (A) Western blot images showing protein expression in foam cells after different treatments, with  $\beta$ -actin as the loading control. Quantified protein levels and relative mRNA expression of SREBP2 (B), LDLR (C), and ABCA1 (D) in the control, bTiO<sub>2</sub>-HA, bTiO<sub>2</sub>-HA-p, and wTiO<sub>2</sub>-HA-p groups with or without 808 nm laser irradiation (1.0 W cm<sup>-2</sup>, 10 min). \* $p < 0.05$ , \*\* $p < 0.01$ .

foam cells to the liver, and it therefore plays a crucial role in regulating cellular cholesterol homeostasis [32]. In our study, the expression of ABCA1 mRNA was significantly upregulated in both the mild PTT and mild PTT + PDT groups, while a slight downregulation trend was observed in the PDT group (Fig. 9D). The upregulation of ABCA1 mRNA correlated with an increase in lipid efflux. Similarly, ABCA1 protein levels were upregulated in the mild PTT and mild PTT + PDT groups. Our results indicated that mild PTT + PDT activated ABCA1-mediated cholesterol efflux by upregulating the expression of ABCA1 on the cell surface. In addition, it has been reported that HSP27 can upregulate the expression of ABCA1 and promote cholesterol efflux by activating the PI3K/PKC $\zeta$ /Sp1 signal pathway in THP-1 macrophage-derived foam cells [17]. Therefore, the upregulated ABCA1 may related with the overexpression of HSP27.

Taken together, our findings indicated that PDT alone caused significant cell death and only decreased negligible 3% of intracellular lipid storage. Mild PTT alone and mild PTT combined with PDT could activate HSP27 expression, therefore reducing 5% and 12.8% lipid deposition, respectively. The overexpressed HSP27 could protect foam cells against apoptosis, which lower the damage induced by ROS. Moreover, HSP27 also upregulated the expression of ABCA1 and promoted cholesterol efflux. Compared with PTT or PDT alone, mild PTT combined with PDT exerts better synergistic effects on intracellular cholesterol metabolism in foam cells, reducing intracellular cholesterol biosynthesis and excess cholesterol uptake via the SREBP2/LDLR pathway and promoting ABCA1-dependent cholesterol efflux. While the mechanism of this synergistic lipid-lowering effect needs further exploration in future. Thus, mild PTT combined with PDT can prevent excessive cholesterol accumulation in foam cells and therefore serve as a potential strategy for AS treatment.

#### 4. Conclusion

We successfully developed multitherapeutic bTiO<sub>2</sub>-HA-p nanoparticles that exert synergistic effects on lipid metabolism in atherosclerotic foam

cells. The synthesized bTiO<sub>2</sub>-HA-p nanoparticles, with the nature of promising photothermal, photodynamic properties and good biocompatibility, can also specifically target macrophage-derived foam cells. Mild PTT generated from bTiO<sub>2</sub>-HA-p nanoparticles not only can protect cells against apoptosis and necrosis, but also activate ABCA1-dependent cholesterol efflux via the upregulation of HSP27 expression. In addition, mild PTT + PDT synergistically reduces intracellular cholesterol biosynthesis, excess cholesterol uptake via the SREBP2/LDLR pathway and promotes cholesterol efflux via ABCA1, significant attenuating lipid accumulation in foam cells. Unlike conventional PTT or PDT, mild simultaneous PTT + PDT using bTiO<sub>2</sub>-HA-p nanoparticles can enhance anti-AS therapeutic effects at a relatively low temperature without causing high levels of cell apoptosis or necrosis. This therapy could be used to alleviate thermal damage to blood vessels *in vivo*, and further studies exploring its potential are warranted. Nevertheless, the present study provides a promising novel strategy for the safe and effective treatment of AS and also lays the foundation for the further exploration of such strategies.

#### CRediT authorship contribution statement

**Ting Dai:** Methodology, Investigation, Formal analysis, Data curation, Writing – original draft. **Wenming He:** Investigation, Conceptualization, Writing – review & editing, Funding acquisition, Resources, Project administration. **Shuangshuang Tu:** Data curation, Formal analysis. **Jinru Han:** Formal analysis, Validation. **Bo Yuan:** Methodology, Validation. **Chenyang Yao:** Methodology, Validation. **Wenzhi Ren:** Conceptualization, Funding acquisition, Supervision, Writing – review & editing. **Aiguo Wu:** Funding acquisition, Resources, Project administration, Supervision, Writing – review & editing.

#### Declaration of competing interest

The authors declare that they have no known competing financial interests or personal relationships that could have appeared to influence

the work reported in this paper.

## Acknowledgements

This work was supported by Natural Science Foundation of China (32171359, 32025021, 31971292), National Key R&D Program of China (2019YFA0405603, 2018YFC0910601), Zhejiang Province Financial Supporting (LGF19C100001, 2020C03110), Key Laboratory of Diagnosis and Treatment of Digestive System Tumors of Zhejiang Province (No. 2019E10020), Zhejiang Provincial Natural Science Foundation of China (LY20H020002), General research program of Zhejiang Provincial Department of health (WKJ-ZJ-2137), Key Scientific and Technological Special Project of Ningbo City (2020Z094) and the Affiliated Hospital of Medical School of Ningbo University Youth Talent Cultivation Program (FYQM-KY-202002). Furthermore, the authors also acknowledge National Synchrotron Radiation Laboratory in Hefei for High End User Cultivation Fund (2020HSC-UE006) and Shanghai Synchrotron Radiation Facility at Line BL15U for X-ray fluorescence imaging.

## Appendix A. Supplementary data

Supplementary data to this article can be found online at <https://doi.org/10.1016/j.bioactmat.2022.01.013>.

## References

- [1] A. Gistera, G.K. Hansson, The immunology of atherosclerosis, *Nat. Rev. Nephrol.* 13 (6) (2017) 368–380.
- [2] A.J. Lusis, Atherosclerosis, *Nature* 407 (6801) (2000) 233–241.
- [3] G. Assmann, P. Cullen, F. Jossa, et al., Coronary heart disease: reducing the risk: the scientific background to primary and secondary prevention of coronary heart disease a worldwide view, *Arterioscler. Thromb. Vasc. Biol.* 19 (8) (1999) 1819–1824.
- [4] I. Tabas, K.E. Bornfeldt, Macrophage phenotype and function in different stages of atherosclerosis, *Circ. Res.* 118 (4) (2016) 653–667.
- [5] K.J. Moore, F.J. Sheedy, E.A. Fisher, Macrophages in atherosclerosis: a dynamic balance, *Nat. Rev. Immunol.* 13 (10) (2013) 709–721.
- [6] A.N. Kharlamov, A.E. Tyurnina, V.S. Veselova, et al., Silica-gold nanoparticles for atheroprotective management of plaques: results of the NANOM-FIM trial, *Nanoscale* 7 (17) (2015) 8003–8015.
- [7] X. Wang, X. Wu, J. Qin, et al., Differential phagocytosis-based photothermal ablation of inflammatory macrophages in atherosclerotic disease, *ACS Appl. Mater. Interfaces* 11 (44) (2019) 41009–41018.
- [8] X. Zhu, H. Wang, L. Zheng, et al., Upconversion nanoparticle-mediated photodynamic therapy induces THP-1 macrophage apoptosis via ROS bursts and activation of the mitochondrial caspase pathway, *Int. J. Nanomed.* 10 (2015) 3719–3736.
- [9] J. Liu, B. Zhou, Y. Guo, et al., SR-A-Targeted nanoplatfor for sequential photothermal/photodynamic ablation of activated macrophages to alleviate atherosclerosis, *ACS Appl. Mater. Interfaces* 13 (25) (2021) 29349–29362.
- [10] I. Tabas, Consequences and therapeutic implications of macrophage apoptosis in atherosclerosis: the importance of lesion stage and phagocytic efficiency, *Arterioscler. Thromb. Vasc. Biol.* 25 (11) (2005) 2255–2264.
- [11] I. Tabas, Macrophage death and defective inflammation resolution in atherosclerosis, *Nat. Rev. Immunol.* 10 (1) (2010) 36–46.
- [12] D. Jaque, L.M. Maestro, B. Del Rosal, et al., Nanoparticles for photothermal therapies, *Nanoscale* 6 (16) (2014) 9494–9530.
- [13] J.A. Inia, E.R. O'Brien, Role of heat shock protein 27 in modulating atherosclerotic inflammation, *J. Cardiovasc. Transl. Res.* 14 (1) (2021) 3–12.
- [14] M. Ghayour-Mobarhan, H. Saber, G.A.A. Ferns, The potential role of heat shock protein 27 in cardiovascular disease, *Clin. Chim. Acta* 413 (1–2) (2012) 15–24.
- [15] C.G. Concannon, A.M. Gorman, A. Samali, On the role of Hsp27 in regulating apoptosis, *Apoptosis* 8 (1) (2003) 61–70.
- [16] T. Zhang, B.H. Wu, O.U. Akakuru, et al., Hsp90 inhibitor-loaded IR780 micelles for mitochondria-targeted mild-temperature photothermal therapy in xenograft models of human breast cancer, *Cancer Lett.* 500 (2021) 41–50.
- [17] H.J. Kuang, G.J. Zhao, W.J. Chen, et al., Hsp27 promotes ABCA1 expression and cholesterol efflux through the PI3K/PKC $\alpha$ /Sp1 pathway in THP-1 macrophages, *Eur. J. Pharmacol.* 810 (2017) 57–62.
- [18] W.Z. Ren, Y. Yan, L.Y. Zeng, et al., A near infrared light triggered hydrogenated black TiO<sub>2</sub> for cancer photothermal therapy, *Adv. Healthc. Mater.* 4 (10) (2015) 1526–1536.
- [19] S.Q. Wang, W.Z. Ren, J.H. Wang, et al., Black TiO<sub>2</sub>-based nanoprobes for T<sub>1</sub>-weighted MRI-guided photothermal therapy in CD133 high expressed pancreatic cancer stem-like cells, *Biomater. Sci.* 6 (8) (2018) 2209–2218.
- [20] W.Z. Ren, M.Z. Iqbal, L.Y. Zeng, et al., Black TiO<sub>2</sub> based core-shell nanocomposites as doxorubicin carriers for thermal imaging guided synergistic therapy of breast cancer, *Nanoscale* 9 (31) (2017) 11195–11204.
- [21] G.D. Mogoşanu, A.M. Grumezescu, C. Bejenaru, et al., Polymeric protective agents for nanoparticles in drug delivery and targeting, *Int. J. Pharm.* 510 (2) (2016) 419–429.
- [22] P. Carloni, E. Damiani, L. Greci, et al., On the use of 1,3-diphenylisobenzofuran (DPBF). Reactions with carbon and oxygen centered radicals in model and natural systems, *Res. Chem. Intermed.* 19 (5) (1993) 395–405.
- [23] S. Garantziotis, R.C. Savani, Hyaluronan biology: a complex balancing act of structure, function, location and context, *Matrix Biol.* 78 (2019) 1–10.
- [24] J. van der Zee, Heating the patient: a promising approach, *Ann. Oncol.* 13 (8) (2002) 1173–1184.
- [25] S.K. Calderwood, Hyperthermia, the tumor microenvironment and immunity, in: Y. Keisari (Ed.), *Tumor ablation: effects on systemic and local anti-tumor immunity and on other tumor-microenvironment interactions*, Springer Netherlands, Dordrecht, 2013, pp. 29–37.
- [26] R.T. Shan, N. Liu, Y.Y. Yan, et al., Apoptosis, autophagy and atherosclerosis: relationships and the role of Hsp27, *Pharmacol. Res.* 166 (2021) 105169.
- [27] H. Kosuge, S.P. Sherlock, T. Kitagawa, et al., Near infrared imaging and photothermal ablation of vascular inflammation using single-walled carbon nanotubes, *J. Am. Heart Assoc.* 1 (6) (2012), e002568.
- [28] L.Y. Huang, Q. Chen, L.H. Yu, et al., Pyropheophorbide- $\alpha$  methyl ester-mediated photodynamic therapy induces apoptosis and inhibits LPS-induced inflammation in RAW264.7 macrophages, *Photodiagnosis Photodyn. Ther.* 25 (2019) 148–156.
- [29] I. Tabas, Apoptosis and plaque destabilization in atherosclerosis: the role of macrophage apoptosis induced by cholesterol, *Cell Death Differ.* 11 (1) (2004) S12–S16.
- [30] K.J. Moore, I. Tabas, Macrophages in the pathogenesis of atherosclerosis, *Cell* 145 (3) (2011) 341–355.
- [31] J. Luo, H.Y. Yang, B.L. Song, Mechanisms and regulation of cholesterol homeostasis, *Nat. Rev. Mol. Cell Biol.* 21 (4) (2020) 225–245.
- [32] D.A. Chistiakov, A.A. Melnichenko, V.A. Myasoedova, et al., Mechanisms of foam cell formation in atherosclerosis, *J. Mol. Med.* 95 (11) (2017) 1153–1165.